Design and Analysis of a Double Membrane Ocean Wave Energy Converter
University of Southern California

Bryce Rogers, David Armendariz, Yifan Xue

May 09, 2022

Abstract

Ocean wave energy is abundantly available yet underutilized. Current wave energy converter (WEC) technologies can not compete with fossil fuels, wind, and solar, and are thus not commercially viable. To contribute to the efforts to expand our renewable energy portfolio to ocean wave energy, a novel two-membrane flexible WEC was designed and tested. A laboratory-scale prototype was constructed, and its power output was measured in single-membrane and double-membrane configurations to determine whether the addition of the second membrane is economical. The findings of this study indicate that the proposed two-membrane WEC is more economical than its single-membrane counterpart.

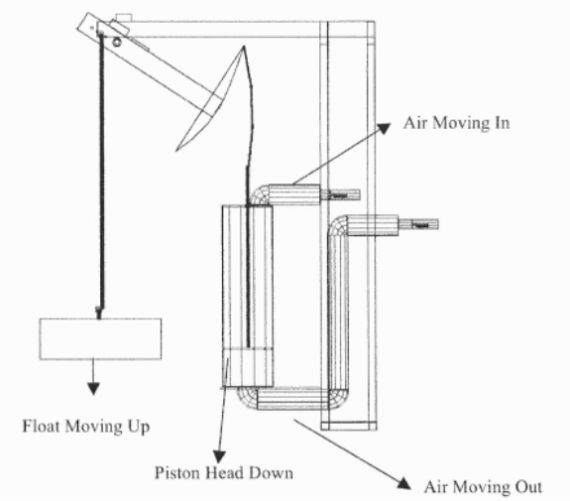

Figure 1: The Ocean Wave Air Piston (US Patent No.: 7,468,563)[5].

1 Introduction

1.1 Motivation

The greenhouse gas emissions associated with energy generation and consumption for human activities must be decreased to mitigate the effects of human-caused climate change. There is currently a global effort to replace emission-intensive fossil fuels with renewable alternatives. Increased exploitation of ocean wave energy could contribute substantially to this effort; according to estimates from the National Oceanic and Atmospheric Administration and the US Department of energy, there is around 2.11 $\pm$ 0.05 TW of wave power available globally (Gunn K, 2012) and 0.26 TW available in the US (US DoE, 2009). There is thus great potential societal value in the development of technologies that can reliably, efficiently, and sustainably convert ocean wave energy into useful work. To this end, this study proposes and tests a novel two-membrane WEC.

Many proposed WEC technologies are currently being studied. The problem that motivates this study is that no existing WEC is yet cost-competetive with the leading sources of electricity, namely fossil fuels, wind, solar. It is therefore valuable to investigate novel designs and innovations that may contribute to the economic viability of WECs, and ultimately expand the global renewable energy portfolio. The goal of this study was to design a novel two-membrane flexible WEC, and determine whether it is more economical than its single-membrane counterpart.

1.2 Background

WEC technologies vary widely in their design. There are two broad classifications: rigid and flexible. Most WECs are rigid WECs, which consist of rigid working surfaces and power take off (PTO) systems. Point absorber buoys and overtopping devices, are common examples of rigid WECs. Figure 1 shows an example of a rigid WEC. This rigid WEC uses the waves to drive a piston, Wells turbines, and generator.

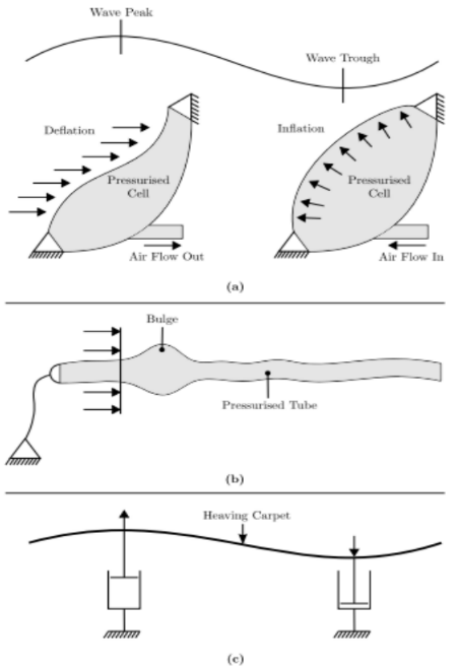

Figure 2: Example WECs.[1]

Flexible WECs employ compliant membranes as their working surfaces, which grants the potential benefits of simplicity of design, low cost [6], low impact on local ecosystems, and the possibility of a dynamically-modifiable resonant response [2]. Flexible WECs are an emerging group of diverse technologies under active research. Proposed flexible WEC designs include compliant wave "carpets" submerged close to the wave surface [2], a submerged air chamber compressed cyclically by a piezoelectric membrane [6], and a floating bag of air compressed cyclically to pump air through a turbine [3]. Figure 2 shows examples of the described flexible WECs under research and development.

Newer approaches to flexible WECs include the use of dielectric elastomer generators (DEG). These devices are electromechanical devices that can generate electrical energy through the deformation of rubber-like dielectric materials under outside forces [4]. DEG devices are an emerging technology in the field of wave power generation due to its high power density (in the order of hundreds of Watts per kilogram) and low material price (a few euros per kilogram), ease of assembly and implementation. Dielectric elastomer materials are also robust and corrosion resistant, making them durable in underwater environments [4]. Figure 3 demonstrates an example of a DEG WEC.

The device in figure 3 is required to be dynamically tuned with the incoming waves. Otherwise its performance drops significantly. However, at an experimental max power of 3.8W, it corresponds to several hundreds of kilowatts at full-scale under similar conditions [4].

Each of these technologies extracts wave energy by leveraging pressure fluctuations to induce membrane deformation and fluid movement. This diversity of WEC design is given by the varied nature of ocean waves and the age of the technologies. Flexible WECs are a young group of

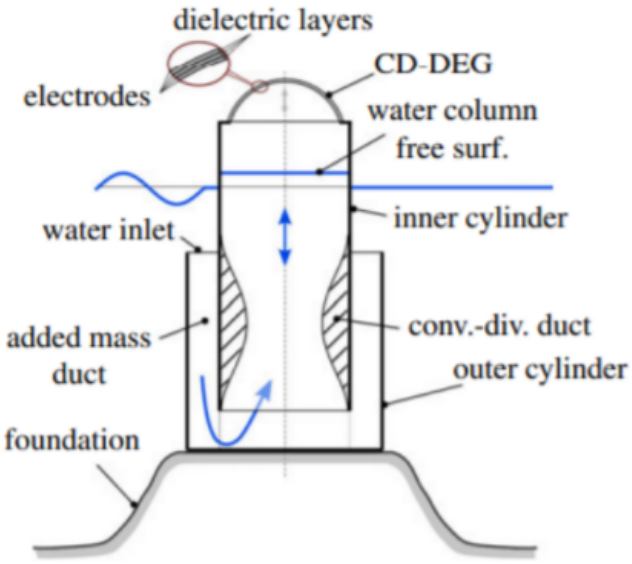

Figure 3: Dielectric Elastomer Generator WEC researched by [4] with an experimental max power of 3.8W

technologies and thus benefit from further investigation of innovations that might make them more economically viable when deployed at full scale. The findings of this study are intended to inform the design of future flexible WECs.

1.3 Theoretical Background and Mathematical Model

The energy contained in an ideal sinusoidal water wave per unit wave crest length and unit wavelength is given by

$$E = \frac{1}{2}\rho g a^2 \qquad [E] = \frac{J/m}{m} \tag{1}$$

where ρ is the water density (assumed constant), g is acceleration due to Earth's gravity, and a is wave amplitude. The time-averaged power of a wave is thus

$$P_i = (\frac{1}{2}\rho g a^2) * \lambda * W_{crest} * f \tag{2}$$

where the i subscript denotes "in", λ is wavelength, W_{crest} is the length of the crest of the wave, and f is the frequency of the wave. It was desired for the ratio of power output of the system to power input from the wave ($\frac{P_o}{P_i}$ to be maximized (i.e. as close to 1 as possible).

The working principle of the system is that wave pressure fluctuations drive membrane deformation, which in turn drives motion of the working fluid within the system. The dynamic pressure

pressure $p(t)$ at depth z below the equilibrium surface of a wave is given by:

$$p(t) = \underbrace{\rho g \frac{\cosh[k(z+H)]}{\cosh[kH]}}_{\text{pressure amplitude}=p_0} \sin(\omega t) \tag{3}$$

where 'dynamic' pressure refers to gauge pressure relative to the hydro-static pressure at depth z, k is the incident wave number, H is the floor-to-surface depth, and ω is the angular frequency of the incident wave. It was assumed that incident waves in this study were ideal, such that Equations 2 and 3 hold.

A mathematical model was developed to establish expectations of system response. The input of the system was the dynamic pressure $p(t)$, and the output of interest was electrical power $P(t)$. Electrical power $P(t)$ can be calculated as a function of the voltage difference $V(t)$ induced across the solenoid according to

$$P(t) = V(t)^2/R \tag{4}$$

where R is the resistance of the solenoid circuit due to the resistivity of the wire. The voltage $V(t)$ induced by a magnet passing through an n loop solenoid can be approximated according to Equation 5

$$V(t) = BnA_s v(t) \tag{5}$$

where B is magnetic field strength, A_s is the cross-sectional area of the solenoid, and $v(t)$ is the velocity of the magnet. It was assumed that the solenoid and magnetic field were ideal. To approximate $v(t)$ given an incident wave with dynamic pressure $p(t)$, the system behavior was modelled by Equation 6, a first order linear ODE:

$$m\dot{v} + cv = A_p \Delta p(t) \tag{6}$$

where m and c are the total inertia and damping of the system respectively, A_p is the area of the piston face, and $\Delta p(t)$ is the pressure difference across the piston. Because water is incompressible, all of the water in the piston tube must accelerate with the piston in order for the piston to move. Therefore m, the total inertia of the dynamic system, was calculated as

$$m = m_{piston} + m_{water} \tag{7}$$

where m_{water} is the mass of the water in the piston tube. Friction and viscous losses in the system were assumed to be negligible, such that the damping c was due entirely to the magnetic resistance that resists the velocity of the magnetic piston through the solenoid induced (according to Lenz's Law). The assumption of a friction less system was not realistic, and was expected to introduce error between predicted and experimental data. It was assumed that the pressures in each box (relative to pressure at rest) were equal and opposite. This assumption corresponds to one box having a peak of the incident wave overhead and the other having a trough. It was also assumed that, due to the elasticity of the membranes, the pressure in each box was 90% of the dynamic pressure of the incident wave at the external membrane surface. Combining these two assumptions yields

$$\Delta P(t) = 2 * (0.9p(t)) \tag{8}$$

Solving Equation 6 for $v(t)$ yields

$$v(t) = \frac{2 * 0.9 * p_0 A_p/m}{\sqrt{(c/m)^2 + \omega^2}} cos(\omega t) \tag{9}$$

		f[Hz]			
		0.25	0.5	1	2
a[cm]	1	22	5.7	1.1	0.083
	3	200	52	10	0.75
	5	**550**	140	28	2.1

Figure 4: Predicted values of power output [mW] as a function of incident wave frequency and amplitude. Darker cell shading indicates higher predicted efficiency $\frac{P_o}{P_i}$

.

where p_0 is the amplitude of the dynamic pressure from Equation 3. To obtain expected values for time-averaged power output P_o, Equations 4, 5, and 9 were combined and various combinations of incident wave amplitude a and frequency f were plugged in. The resulting table of expectations is provided in Figure 4. The table is shaded according to predicted efficiency $\frac{P_o}{P_i}$; the highest predicted efficiency was 19% ($a = 1cm, f = 0.25Hz$), and the lowest was 0.02% ($a = 5cm, f = 2Hz$). The limitations of the mathematical model and agreement of expectations with the results is detailed in the Results and Discussion section.

2 Materials and Methods

The experimental system consisted of two membrane-enclosed volumes of water separated by a freely sliding piston. Pressure fluctuations induced piston motion, which in turn generated electricity via an electromagnetic PTO, as described below.

2.1 System Design: Mechanical

The system consisted of two water-filled acrylic boxes connected by a tube. Each box had a rectangular orifice on its top, over which a rubber membrane was secured. The membrane was secured by compressing it between the top of the box and an acrylic frame using a bolt pattern, For the membrane material, TheraBand Yellow Latex band was selected due its low energy losses over a wide deformation range[7]. During single-membrane tests, the membrane of one box was replaced with a rigid top. The box-tube assembly is shown in Figure 7.

Each box had a circular hole in one side into which a cylindrical insert was glued. Each end of the tube was inserted into one of these inserts, with an o-ring between the tube end and insert to ensure water-tightness. A piston was manufactured with a loose fit with the 1.5in ID of the tube, such that it could slide freely. A slot was made inside the piston to contain four magnets, as shown in Figure 8. These magnets are part of the electromagnetic PTO system, discussed in the next section.

Two narrow flexible tubes were inserted through holes drilled in the side of each box. The other end of each tube was connected to a differential pressure sensor, which converts a pressure difference between its two ports into a voltage signal. As an overview, the experiment schematics for the single membrane system is shown in 5, and the experiment schematics for the double membrane system is shown in 6.

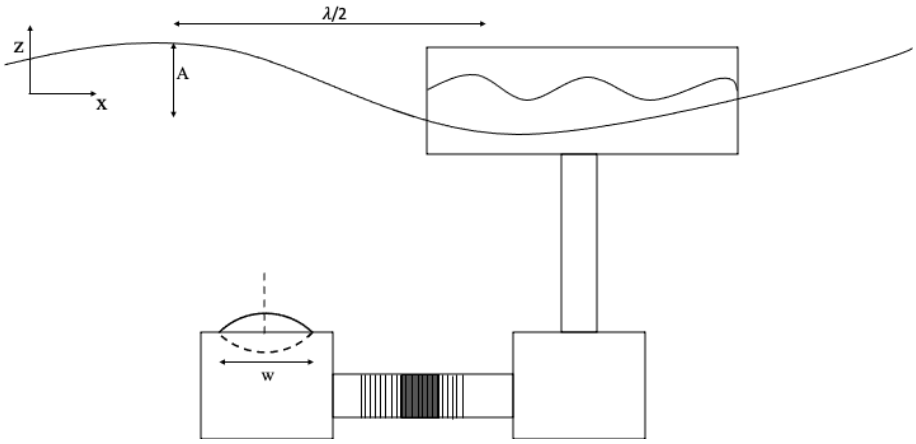

Figure 5: Experiment schematics for the single membrane system.

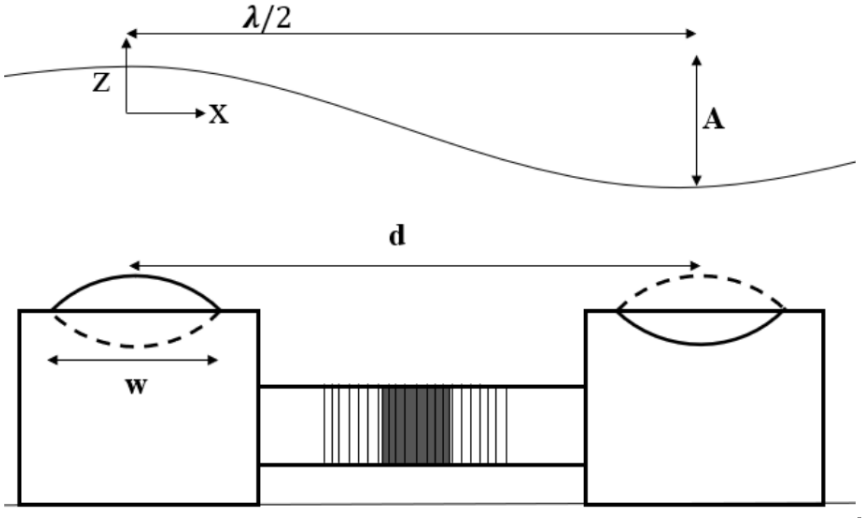

Figure 6: Experiment schematics for the double membrane system.

2.2 System Design: Electrical

The magnets used were N52 1.26 inch x 1/8 inch Circular Neodymium Disc Magnets. The piston tube was wrapped in copper wire to form a 4 inch long solenoid with approximately 3000 turns. Either end of this wire was attached to an NI DAQ that read voltage across the solenoid as a function of time. This voltage data was collected using LabVIEW and used to calculate output power.

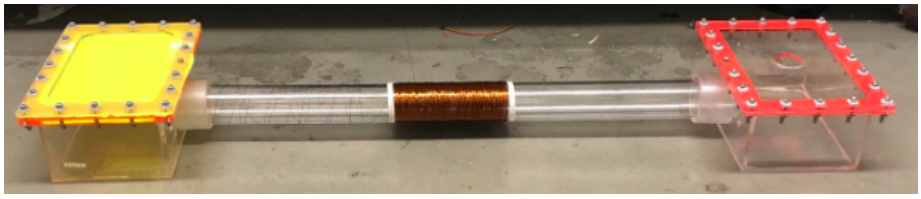

Figure 7: Assembly of boxes, piston tube, and solenoid in single-membrane configuration (the box on the right has a rigid top).

An NI DAQ and LabView were also used to record the voltage readings of the differential pressure sensor simultaneously. Although voltage was the data of primary interest, the pressure difference between the boxes was also measured as a source of redundancy and comparison.

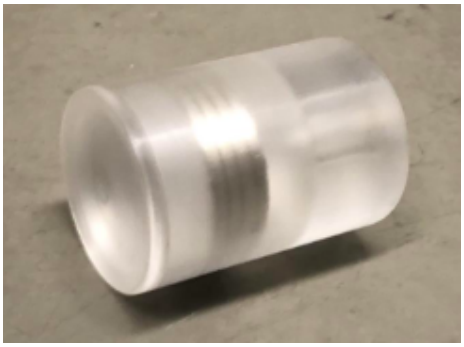

Figure 8: Piston and lid with magnets shown inside.

2.3 Manual Wave Generator

The team originally proposed to use a custom wavemaker built using a stepper motor NEMA23, along with a custom stepper motor traverser offered by the lab. A pedal the width of the largest width of the water tank was made out of an aluminum plate to generate waves. The pedal was connected to a stepper motor traverser controlled by LabVIEW and Anaheim Automation control 'black box' to make waves at different frequencies. However, the motor torque turned out to be insufficient and the waves generated using the wavemaker failed to provide sufficient energy to move the piston. As a result, we decided to generate waves manually using the same pedal.

To do this, we placed the pedal in the water parallel to the cross section of the tank and moved the pedal back and forth periodically within a certain distance. A metronome (using beats per minute) was used to assist us in making waves with consistent frequencies. The amplitude of the waves we made was controlled by the distance the pedal was pushed in one cyclic movement. Waves of varying frequency were made. Such frequencies included 45, 60, 75, 90, 105 beats per minute. The amplitude was varied by min, medium and max, depending on how far the pedal was pushed back and forth.

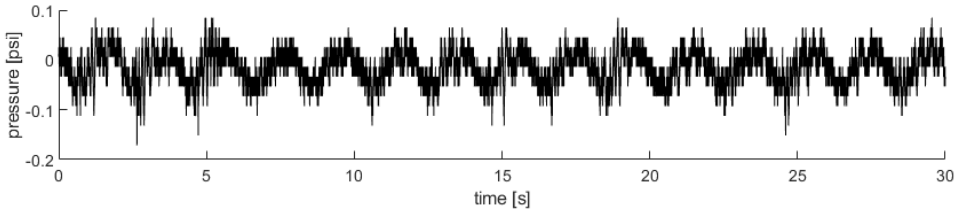

(a) Pressure waveform

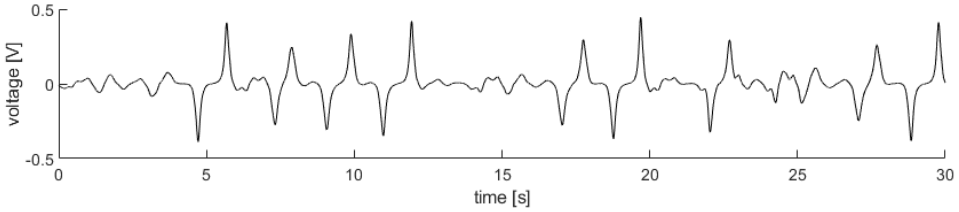

(b) Voltage waveform

Figure 9: Pressure and voltage waveforms collected during a single case.

2.4 Parameters Summary

Relevant parameters of the hardware design and experimental setup are summarized in Table 2.4.
Table 1: Hardware Design Parameters

Name	Parameter	Value	Unit
Wave Frequency	f	0.125 - 1.5	Hz
Box Length	L_b	20.0	cm
Box Width	W_b	12	cm
Box Height	H	10.0	cm
Membrane Slit Length	L_m	18	cm
Membrane Slit Width	w	10.5	cm
Acrylic Thickness	t	1/8	in
Cylinder Channel Inner Diameter	D	1.5	in
Membrane Separation	d	70	cm
Solenoid Length	L_s	12.5	cm
Total Wire Length	L_w	25.0	m
Magnetic Field Strength	B	7100	G

3 Results and Discussion

The raw data collected for each consisted of pressure and voltage time series. Representative waveforms are shown below for the case ($f = 0.5$Hz,$a = 5.5$cm):

The noise of the pressure waveforms was substantial compared to the pressure magnitudes themselves. The voltage waveforms were periodic, as expected, but they diverged from the ideal sinusoidal behavior that was assumed in the model.

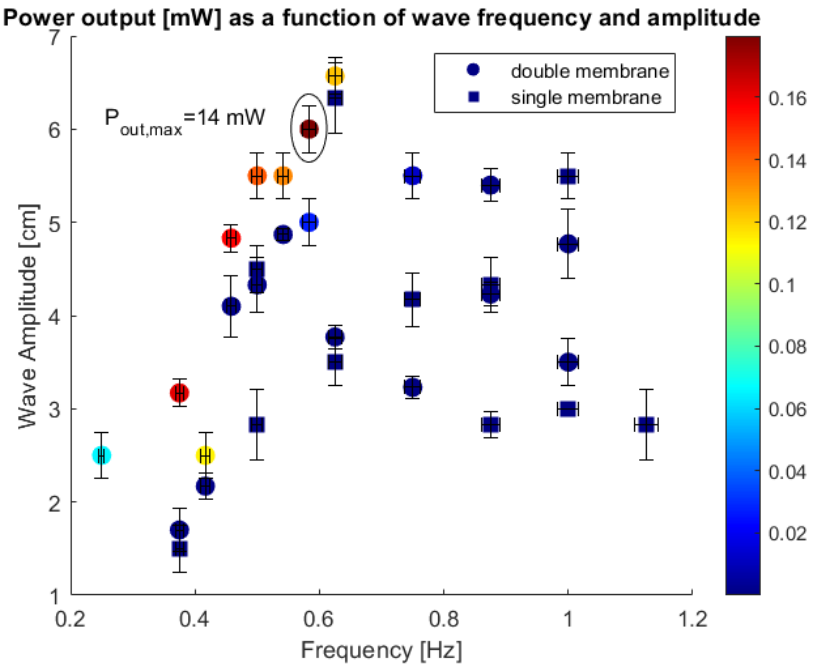

Figure 10: Output power as a function of incident wave amplitude and frequency.

Power output (represented by color, more red corresponds to higher power) as a function of a and f is presented in Figure 10. Power output increased strongly as a function of a, as was predicted by the model. This seems logical given that P_i is proportional to a^2. However unlike the model, which predicted that power output would increase as f decreased, there was a 'sweet spot' for f around 0.5Hz. This is likely due to the geometry of the system, and the model assumption that the pressure in each box is always equal and opposite. In reality, the relative position along the wave of the boxes matters. When the wavelength was very long, the two membranes were not sufficiently out of phase with each other, and thus their work was not perfectly constructive.

Plots of energy conversion efficiency (P_o/P_i) are plotted below vs. the dimensionless quantities w/λ and $d/lambda$. These quantities characterize the geometry of the system relative to the incident wave geometry. Unexpectedly, these plots do not reveal clear relationships between efficiency and w/λ or $d/lambda$. This is likely due to the nonidealities in the system setup, particularly wave reflection. The water channel was approximately 2m long, which was not much longer than a single wavelength for some cases. The causes substantial wave reflections and interference with the boxes that caused the results to diverge significantly from the more ideal behavior of a longer water channel with more end damping.

4 Conclusion

By comparing the single membrane setup to the double membrane setup, we concluded that the double membrane system we designed sufficiently outperformed the single membrane setup such

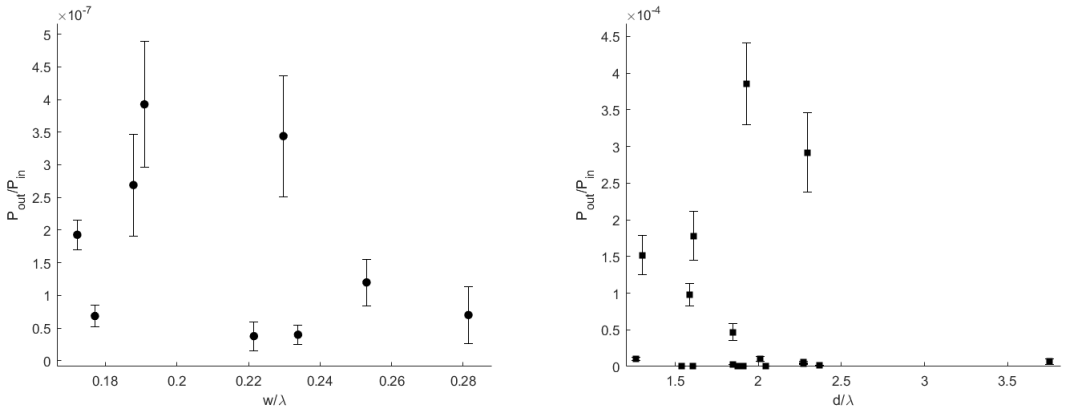

(a) Efficiency vs. w/λ (b) Efficiency vs. d/λ

Figure 11: Power conversion efficiency with different ratios of system geometry to wave geometry

that it is the more economical configuration. The double membrane's potential in competing with existing single membrane wave energy take off systems developed by other researchers. However, a lot of future works still need to be done before the product may be commercialized.

First of all, power loss during power transmission from the bottom of the ocean to the cities and towns in the coastal areas is tremendous. In our experiment, we use copper wires as current transmission medium. The resistance of our copper wire is nearly negligibly and as a result, the power loss during the transmission does not affect the outputs of the experiments. However, in real life applications, when the cable is 100 or even 1000 miles long, things are not going to work the same as in the lab experiment. Therefore, we recommend studying an efficient way to take current from the wave energy converter to nearby cities as a next step of the research.

In addition to that, in the lab environment, the wave generated are relatively small and makes no threat to the acrylic boxes. However, when commercializing the design, we need to find better materials that can resist the wave corrosion instead of acrylic.

5 Acknowledgements

Our team is thankful to Professor Mitul Luhar for his advice and provision of water channel acces. We also thank Professors Darek Bogucki, Robert Antypas, and Geoffrey Spedding for their guidance, and AME Lab Manager Rod Yates for his constant technical support.

6 Appendix

6.1 Uncertainty Calculations

The uncertainty of voltage, pressure, and solenoid resistance were equal the $+-\frac{1}{2}$ of the smallest division of the each digital measurement: 0.1 mV, 0.001psi, and 0.1 Ω, respectively. The uncertainty of the wavelength and amplitude was taken to be the standard deviation of 3 measurements take at different times during each respective 30 second test interval. The uncertainty of the measurements of membrane width w and membrane separation d were assumed to be 0. The wave frequency uncertainty was estimated as $+-\frac{1}{2}$ during the 30 second test interval. The uncertainties of calculated quantities were determined using relative uncertainty:

$$\Delta P_o = P_o\sqrt{(\frac{2\Delta V}{V})^2 + (\frac{\Delta R}{R})^2} \qquad \Delta(\frac{w}{\lambda}) = (\frac{w}{\lambda})\frac{\Delta\lambda}{\lambda}$$

$$\Delta P_i = P_i\sqrt{(\frac{2\Delta a}{a})^2 + (\frac{\Delta\lambda}{\lambda})^2 + (\frac{\Delta f}{f})^2} \qquad \Delta(\frac{d}{\lambda}) = (\frac{d}{\lambda})\frac{\Delta\lambda}{\lambda}$$

$$\Delta(\frac{P_o}{P_i}) = (\frac{P_o}{P_i})\sqrt{(\frac{\Delta P_o}{P_o})^2 + (\frac{\Delta P_i}{P_i})^2}$$

References

[1] Ieuan Collins, Mokarram Hossain, Wulf Dettmer, and Ian Masters. Flexible membrane structures for wave energy harvesting: A review of the developments, materials and computational modelling approaches. *Renewable and Sustainable Energy Reviews*, 151:111478, 2021.

[2] Nicolas Desmars, Joel Tchoufag, Davood Younesian, and Reza Alam. Interaction of surface waves with an actuated submerged flexible plate: Optimization for wave energy extraction. *Journal of Fluids and Structures*, 2018.

[3] A. Kurniawan, J. R. Chaplin, D. M. Greaves, and M. Hann. Wave energy absorption by a floating air bag. *Journal of Fluid Mechanics*, 812:294–320, 2017.

[4] Giacomo Moretti, Miguel Santos Herran, David Forehand, Marco Alves, Henry Jeffrey, Rocco Vertechy, and Marco Fontana. Advances in the development of dielectric elastomer generators for wave energy conversion. *Renewable and Sustainable Energy Reviews*, 117:109430, 2020.

[5] Arun Ramadass. Air piston approach to wave power generation. 2010.

[6] Michele Righi, Giacomo Moretti, David Forehand, Lorenzo Agostini, Rocco Vertechy, and Marco Fontana. A broadbanded pressure differential wave energy converter based on dielectric elastomer generators. *Nonlinear Dynamics*, 2020.

[7] Chen Yi. Dielectric elastomer materials for large-strain actuation and energy harvesting: a comparison between styrenic rubber, natural rubber and acrylic elastomer. *Smart materials and structures*, 2019.